Evolution of binary black holes in self gravitating discs: dissecting the torques

C. Roedig[1]⋆, A. Sesana[1], M. Dotti[2], J. Cuadra[3], P. Amaro-Seoane[1,4] and F. Haardt[5]

[1] *Max-Planck-Institut für Gravitationsphysik, Albert Einstein Institut, Am Mühlenberg 1, 14476 Golm, Germany*
[2] *Università di Milano Bicocca, Dipartimento di Fisica, G. Occhialini, Piazza della Scienza 3, I-20126, Milano, Italy*
[3] *Departamento de Astronomía y Astrofísica, Pontificia Universidad Católica de Chile, 7820436 Macul, Santiago, Chile*
[4] *Institut de Ciències de l'Espai (CSIC-IEEC), Campus UAB, Torre C-5, parells, 2ⁿᵃ planta, ES-08193, Bellaterra, Barcelona, Spain*
[5] *Dipartimento di Scienza e Alta Tecnologia, Università dell'Insubria, via Valleggio 11, 22100 Como, Italy*

ABSTRACT

We analyse three-dimensional smoothed particle hydrodynamics simulations of the evolution of initially quasi-circular massive black hole binaries (BHBs) residing in the central hollow (*cavity*) of massive self-gravitating circumbinary discs. We perform a set of simulations adopting different thermodynamics for the gas within the cavity and for the 'numerical size' of the black holes. Aimed at understanding the physical roots of the secular evolution of the binary, we study the interplay between gas accretion and gravity torques in changing the binary elements (semi-major axis and eccentricity) and its total angular momentum budget. We pay special attention to the gravity torques, by analysing their physical origin and location. We show that (i) the BHB eccentricity grows due to gravity torques from the inner edge of the disc, independently of the accretion and the adopted thermodynamics; (ii) the semi-major axis decay depends not only on the gravity torques but also on their subtle interplay with the disc-binary angular momentum transfer due to accretion; (iii) the spectral structure of the gravity torques is predominately caused by disc edge overdensities and spiral arms developing in the body of the disc; (iv) the net gravity torque changes sign across the BHB corotation radius: gas inside this radius exerts a net positive torque, while streams located outside this radius (but within the cavity) exert a net negative torque. The relative importance of the two might depend on the thermodynamical properties of the instreaming gas and is crucial in assessing the disc–binary angular momentum transfer; (v) the net torque manifests as a purely kinematic effect as it stems from the low density cavity, where the material flows in and out in highly eccentric orbits. Thus both accretion onto the black holes and the interaction with gas streams inside the cavity must be taken into account to assess the fate of the binary.

Key words: Black hole physics – Accretion, accretion discs – Numerical – Hydrodynamics

1 INTRODUCTION

In the currently favoured hierarchical framework of structure formation (White & Rees 1978), galaxies evolve through a complex sequence of merger and accretion events, and the existence of massive black holes (BHs) at their centres is nowadays a well established observational fact (see Gültekin et al. 2009, and references therein). By combining together these two pieces of information, the formation of a large number of massive black hole binaries

(BHBs), following galaxy mergers throughout cosmic history, is a natural consequence of the structure formation process (Begelman et al. 1980). Although this is corroborated by several observed quasar pairs at a ∼ 100kpc projected separation (Hennawi et al. 2006; Myers et al. 2007, 2008; Foreman et al. 2009; Shen et al. 2011), and by few ≲ kpc dual accreting BHs embedded in the same galaxy (e.g. Komossa et al. 2003; Fabbiano et al. 2011), identification of gravitationally bound BHBs in galaxy centres remains elusive (for an up-to-date review on the candidates see Dotti et al. 2012, and references therein).

Even though observationally there is little evidence for

⋆ E-mail: croedig@aei.mpg.de

their existence, much theoretical work has focused lately on Keplerian massive BHBs residing in galactic nuclei. One reason is that a deep understanding of the interplay between BHBs and their dense (stellar and gaseous) environment is required to predict robust signatures that may allow their identification. Additionally, it is still unclear how the gap between the two theoretically well understood stages of BHB evolution is bridged: (i) the dynamical friction driven stage, when the two BHs spiral in toward the centre of the merger remnant down to pc separations and (ii) the final inspiral driven by gravitational waves (GWs), which become efficient when the two BHs are at a separation $\lesssim 10^{-2}$ pc. Both dense stellar and gaseous environments have been shown to be effective in extracting the binary energy and angular momentum (see, e.g., Escala et al. 2005; Dotti et al. 2007; Cuadra et al. 2009; Khan et al. 2011; Preto et al. 2011), likely driving the system to final coalescence (an extensive discussion on the fate of sub-parsec BHBs can be found in Dotti et al. 2012). Scenarios involving cold gas are particular appealing not only because they might produce distinctive observational signatures, but also because cold gas dominates the baryonic content in most galaxies at redshifts higher than one, providing a natural reservoir of energy and angular momentum to drive the BHB towards coalescence.

Numerical simulations of wet galaxy mergers (e.g., Mihos & Hernquist 1996; Mayer et al. 2007) have led to the following picture for the post merger evolution. Cold gas is funnelled to the central ≈ 100 pc by gravitational instabilities, where it forms a puffed, rotationally supported circumnuclear disc. Disc-like structures are actually observed in ULIRGs which are thought to be gas rich post-merger star-forming galaxies (e.g., Sanders & Mirabel 1996; Downes & Solomon 1998; Davies et al. 2004a,b; Greve et al. 2009). In the models, the two nuclear BHs efficiently spiral to sub-pc scales owing to dynamical friction against the massive circumnuclear disc (Dotti et al. 2007), eventually opening a cavity (or hollow) in the gas distribution (Goldreich & Tremaine 1980). The subsequent evolution of the system is determined by the efficiency of energy and angular momentum transfer between the BHB and its outer circumbinary disc.

The investigation of coupled disc–binary systems has a long-standing tradition in the context of planetary dynamics (Goldreich & Tremaine 1980; Lin & Papaloizou 1986; Ward 1997; Bryden et al. 1999; Lubow et al. 1999; Nelson et al. 2000), where the focus usually lies on the extreme mass ratio situation, i.e., a star surrounded by a circumstellar disc, with a planetary companion embedded in it. The comparable mass case has also been extensively investigated in the context of binary star formation (Artymowicz & Lubow 1994; Bate & Bonnell 1997; Günther & Kley 2002; Günther et al. 2004), where a boost of activity has been triggered by imaging of nearby young binary stars embedded in hollow circumbinary discs (Dutrey et al. 1994). More recently, the techniques adopted in these fields have been applied to the BHB case. In the last decade, several investigations were devoted to the study of comparable mass BHBs evolving in circumbinary discs, exploiting a variety of analytical and numerical techniques (Ivanov et al. 1999; Armitage & Natarajan 2002, 2005; Hayasaki et al. 2007, 2008; MacFadyen & Milosavljević 2008; Hayasaki 2009; Cuadra et al. 2009; Lodato et al. 2009; Nixon et al.

2011; Roedig et al. 2011; Shi et al. 2011). However only few of them focused on the details of the dynamical disc–binary interplay. MacFadyen & Milosavljević (2008) (hereinafter MM08) made use of two-dimensional grid-based hydrodynamical simulation to study a BHB embedded in a thin α-disk (Shakura & Sunyaev 1973). They showed that the gas flowing through the cavity increases the energy and angular momentum transfer between the disc and the binary. Shi et al. (2011) (hereinafter S11) confirmed that result using full 3D magnetohydrodynamics (MHD) simulations. However, in both studies the BHB was on a fixed circular orbit, the central region of the disc (i.e. within twice the binary separation) was excised from the computational domain, and the disc self-gravity was neglected.

We employ full 3D smoothed particle hydrodynamical (SPH) simulations to study the interaction between BHBs and their surrounding discs. Our goal is to give a detailed description of the coupled disc–binary dynamics, paying particular attention to the competing effects of disc–binary gravitational torques and gas accretion onto the BHs in the evolution of the binary angular momentum budget. We simultaneously evolve the disc and the two BHs in a self-consistent way. This enables us to separately investigate the effect of gravitational torques coming from different disc regions and to directly link different physical mechanisms (gravitational torques and accretion) to the evolution of individual quantities describing the binary (mass, mass ratio, semi-major axis and eccentricity). Our approach allows a broader understanding of the coupled dynamics with respect to previous studies (MM08, S11), where the binary was modelled as a fixed forcing quadrupolar potential and the central region was excised. Thanks to the relative low computational cost of the SPH implementation we could perform different runs varying physical and numerical prescriptions that may play a relevant role in the disc–binary energy and angular momentum exchanges. Specifically, we checked the possible dependence of our results on the 'numerical size' of the two BHs (i.e., their sink radii, see next Section), and on the adopted equation of state (EoS) for the gas within the central cavity.

The paper is structured as follows: we first describe the numerical setup and initial conditions in Section 2, then we show the importance of both accretion and gravitational torques on the binary evolution in Section 3. We study in detail the origin and strength of the mutual disc–binary gravitational torques in Section 4 highlighting the influence of the thermodynamics prescription. In Section 5 we briefly discuss the temporal behaviour and the spatial geometry of the accretion, speculating on the evolution of the binary mass ratio and BH individual spins. Finally, we compare our results to previous work in Section 6 and discuss the implications of our findings and give our conclusions in Section 7.

2   SIMULATIONS

The model and numerical setup of this work is closely related to that of Roedig et al. (2011) and Cuadra et al. (2009), hence we only outline the key aspects in the following, and refer the reader to these two papers for further details.

We simulate a self-gravitating gaseous disc of mass $M_d = 0.2\,M$ around two BHs of combined mass $M =$
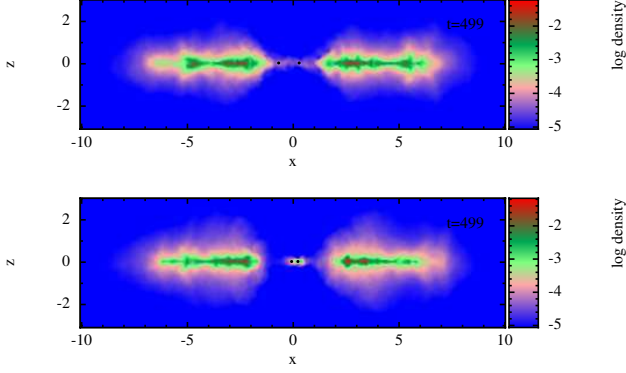
Figure 1. Relaxed meridional density maps of the disc for the *adia* (top) and *iso* (bottom) runs; the black dots indicate the BHs, the axis are in units of the binary semi-major axis a. Note that this is not an azimuthal average but a vertical slice of the disc.
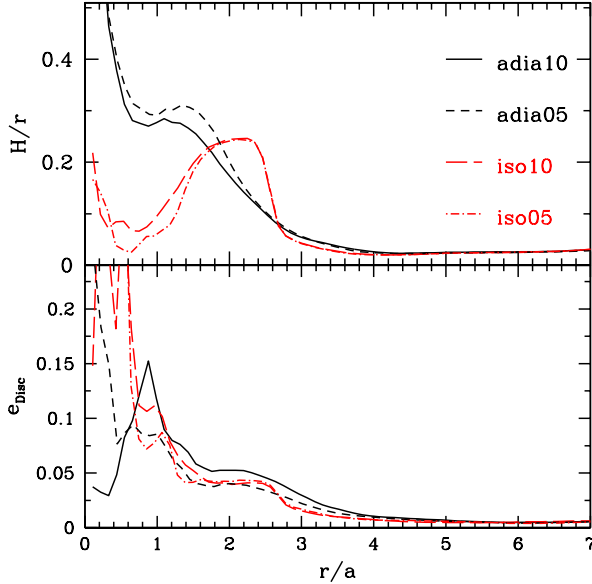

Figure 2. Time and azimuth-averaged values of the disc scale-height H/r and the disc eccentricity $e_{\rm disc}$ as a function of radius for the different simulations.

$M_1 + M_2$, mass ratio $q = M_2/M_1 = 1/3$, eccentricity e and semi-major axis a, using the SPH-code GADGET-2 (Springel 2005) in a modified version that includes sink-particles which model accretion on to the BHs (Springel et al. 2005; Cuadra et al. 2006). Moreover, the orbit of the BHB is followed very accurately by using a fixed small time-step and summing up directly the gravitational force from every other particle in the simulation (Cuadra et al. 2009). The disc, which is co-rotating with the BHs, radially extends to about $7a$, contains a circumbinary cavity of radial size $\sim 2a$ and is numerically resolved by 2 million particles. The numerical size of each BH is denoted as $r_{\rm sink}$, the radius below which a particle is accreted, removed from the simulation, and its momentum is added to the BH (Bate et al. 1995). The gas in the disc is allowed to cool on a time scale proportional to

Table 1. Initial parameters and names of the runs in unitlengths of the code.

Model	$r_{\rm sink}$	Cavity EoS	Disc EoS
adia10	0.1	adiabatic+β	adiabatic +β
iso10	0.1	isothermal	adiabatic +β
adia05	0.05	adiabatic+β	adiabatic +β
iso05	0.05	isothermal	adiabatic +β

the local dynamical time of the disc $t_{\rm dyn} = f_0^{-1} = 2\pi/\Omega_0$, where $\Omega_0 = (GM_0/a_0^3)^{1/2}$ is the initial orbital frequency of the binary[1]. To prevent it from fragmenting, we force the gas to cool slowly, setting $\beta = t_{\rm cool}/t_{\rm dyn} = 10$ (Gammie 2001; Rice et al. 2005). We use two different treatments for the thermodynamics inside the cavity, denoted as *adia* and *iso*, respectively. In the *adia* runs, the gas within the cavity is allowed to both cool via the β prescription and to heat up adiabatically, as it is the remainder of the disc (Cuadra et al. 2009). In the *iso* runs, we define a threshold radius $r_{\rm cavity} = 1.75a$, below which the gas is treated isothermally, meaning that the internal energy per unit mass is set to be $u \approx 0.14(GM/R)$ (Roedig et al. 2011).

As initial conditions we use a relaxed snapshot from Cuadra et al. (2009) taken at their $t = 500\Omega_0^{-1}$ (see Roedig et al. (2011), Section 2.1)[2] . The nomenclature of the runs and the parameters used are listed in Tab. 1. Each run is evolved for ≈ 90 binary orbits, and we store the output in single precision ~ 6 times per orbit. We also closely track accretion by storing the position and velocity of the two BHs and of each accreted particle at the time the latter crosses the sink radius. For both prescriptions (*adia* and *iso*) we show the relaxed density configurations sliced along the meridional plane in Fig. 1 (see also Figs. 8–9 for a face-on view)[3] and the measured, time-averaged values for both the scale height of the disc H/r, and the eccentricity of the disc $e_{\rm disc}$ in Fig. 2. H is taken to be the height above and below the disc-orbital plane in which 70% of the mass inside the annulus $(r, r + dr)$ is found. In their bodies (i.e. at $r > 2a$), the discs may be considered thin, as shown in the upper panel of Fig. 2, with a maximum thickness $H/r \approx 0.2$, and quasi circular (lower panel of Fig. 2). Generally, we can consider the physics to be resolved if the smoothing length h is smaller than the characteristic lengthscale: radially the criterion $h/r \ll 1$ is achieved well: $h/r \in (0.005, 0.2)$; whereas vertically the resolution in the main body of the disc is about $h/H \in (0.1, 0.25)$ [4].

Unless otherwise stated, we will present all the relevant quantities in the natural units of the simulation by setting $G = M_0 = a_0 = 1$. It follows that also the initial circular velocity of the binary is $V_{c,0} = 1$ and its initial period $P_0 = 2\pi$. We will then discuss the astrophysical implications of

---

[1] Subscripts 0 refer to the initial values of any parameter.
[2] Notice that in the remainder of this article we refer to the time of this snapshot as $t = 0$.
[3] Plots made using SPLASH (Price 2007).
[4] The specified values are not met inside the cavity, due to the relatively small quantity of gas. This yields $h/H \in (1, 4)$ for $r < 1.5\,a$.
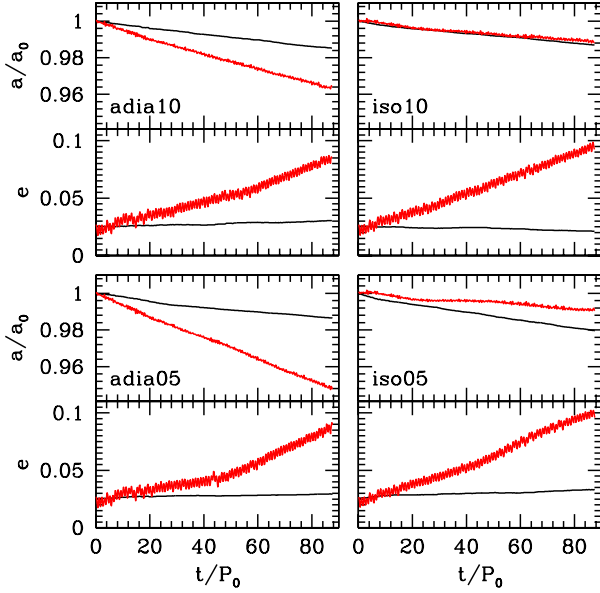
Figure 3. Semimajor axis (top panel in each plot) and eccentricity (bottom panel in each plot) evolution for all the four runs. In each panel, the red line represents the full evolution directly taken from the simulation whereas the black line is the equivalent evolution when considering the energy and angular momentum exchanges due to accreted particles only.

our findings by scaling them to fiducial astrophysical BHB systems.

3   BINARY EVOLUTION: CAUSES

For each of the four runs, we measure the two primary orbital elements: eccentricity e and semi-major axis a. Their evolution is shown by the red lines in Fig. 3. In all four runs, we find $\dot{a}(t) < 0$ and $\dot{e}(t) > 0$. While the eccentricity evolution is largely independent on the sink radius value and the adopted EoS within the cavity, the orbital shrinking is much faster in the *adia* runs, in which the binary shrinks by $4 - 5\%$ over 90 orbits. Conversely, in the *iso* runs, the two BHs get only about 1% closer. Linear extrapolation of such results at face value implies binary coalescence on a timescale of $\sim 2000 P_0$ and $\sim 10^4 P_0$ for the *adia* and the *iso* runs, respectively. Whereas, assuming a constant eccentricity growth rate, the limiting value predicted by Roedig et al. (2011) would be reached in less than $\sim 1000 P_0$.

3.1   Gravitational torque and accretion contribution to the angular momentum budget

Being interested in the physical mechanisms driving the binary evolution, we firstly identify two distinct processes:

(i) the gravitational torques exerted by the gaseous particles onto each individual BH, $\mathbf{T}_G$ (gravity torque)

(ii) the accretion of instreaming particles crossing either BH sink radius, $(d\mathbf{L}/dt)_{\mathrm{acc}}$ (accretion torque).

Conservation of the total angular momentum in the simulations implies

$$\frac{d\mathbf{L}}{dt} = \mathbf{T}_G + \frac{d\mathbf{L}}{dt}_{\mathrm{acc}}, \tag{1}$$

where $\mathbf{L}$ is the BHB orbital angular momentum vector [5]. All vectors are computed with respect to a Cartesian reference frame centred in the BHB centre of mass (CoM)[6]; the binary initially lies in the x–y plane with angular momentum oriented along the positive z axis. In our SPH simulations, $\mathbf{T}_G$ can be computed at each snapshot by direct summation of individual particle torques onto each BH yielding

$$\mathbf{T}_G = \sum_{j=1}^{N} \sum_{k=1}^{2} \mathbf{r}_k \times \frac{GM_k m_j(\mathbf{r}_j - \mathbf{r}_k)}{|\mathbf{r}_j - \mathbf{r}_k|^3}, \tag{2}$$

where j runs over all N gas particles, k identifies the two BHs, $\mathbf{r}$ are position vectors, and m and M denote particle and BH masses respectively. On the other hand, $(d\mathbf{L}/dt)_{\mathrm{acc}}$ can be computed by assuming instantaneous linear momentum conservation of each accreted particle yielding $\Delta\mathbf{L} = \mathbf{r}_k \times m_j\mathbf{v}_j$. Here $\mathbf{r}_k$ is the position vector of the accreting BH at the moment of swallowing the particle, and $\mathbf{v}_j$ is the particle velocity vector. Numerically, we can evaluate the binary angular momentum change $\Delta\mathbf{L}$ at each snapshot by writing Eq. (1) in the form

$$\Delta\mathbf{L} = \mathbf{T}_G \Delta t + \sum_{\Delta t} \mathbf{r}_k \times m_j\mathbf{v}_j, \tag{3}$$

where Δt is the interval between two subsequent snapshots, and the sum runs over all the accretion events occurring in this time lapse.

We use Eq. (3) to assess the relative importance of gravitational torques and accretion in the evolution of the system. In Fig. 4, we plot the evolution of the x, y, z components of the angular momentum $\mathbf{L}$ as directly evaluated from the positions and velocities of the two BHs stored in the simulation outputs (red), together with the relative changes due to accretion (black dotted) and gravity torques (black dashed) according to Eq. (3). The solid black line is the sum of the latter two which should overlap with the red line if our decomposition is sufficiently accurate and these are the only two physical processes determining the binary evolution. For comparison, in simulation units, the initial binary angular momentum is ≈ 0.18. The L_x and L_y components are almost constant, showing fluctuations at the 10^{-4} level. The mismatch between the red and the solid black lines here is because simulation outputs are in single precision, i.e. accurate to the fourth digit, which is the fluctuation level of the computed quantity. On the contrary, the L_z component changes up to a 10^{-2} absolute level (i.e., about 5% of the initial value), and in this case we see very good agreement between the two lines. Note that in three of the runs, the overall angular momentum grows over time, even though a shrinks and e increases. This counter intuitive result is due

---

[5] Throughout the paper we will denote all vectorial quantities in boldface.

[6] The binary CoM slightly wiggles around the total binary–disc CoM. As a cross check, we also computed all the relevant quantities with respect to the latter, finding no significant difference in the results.
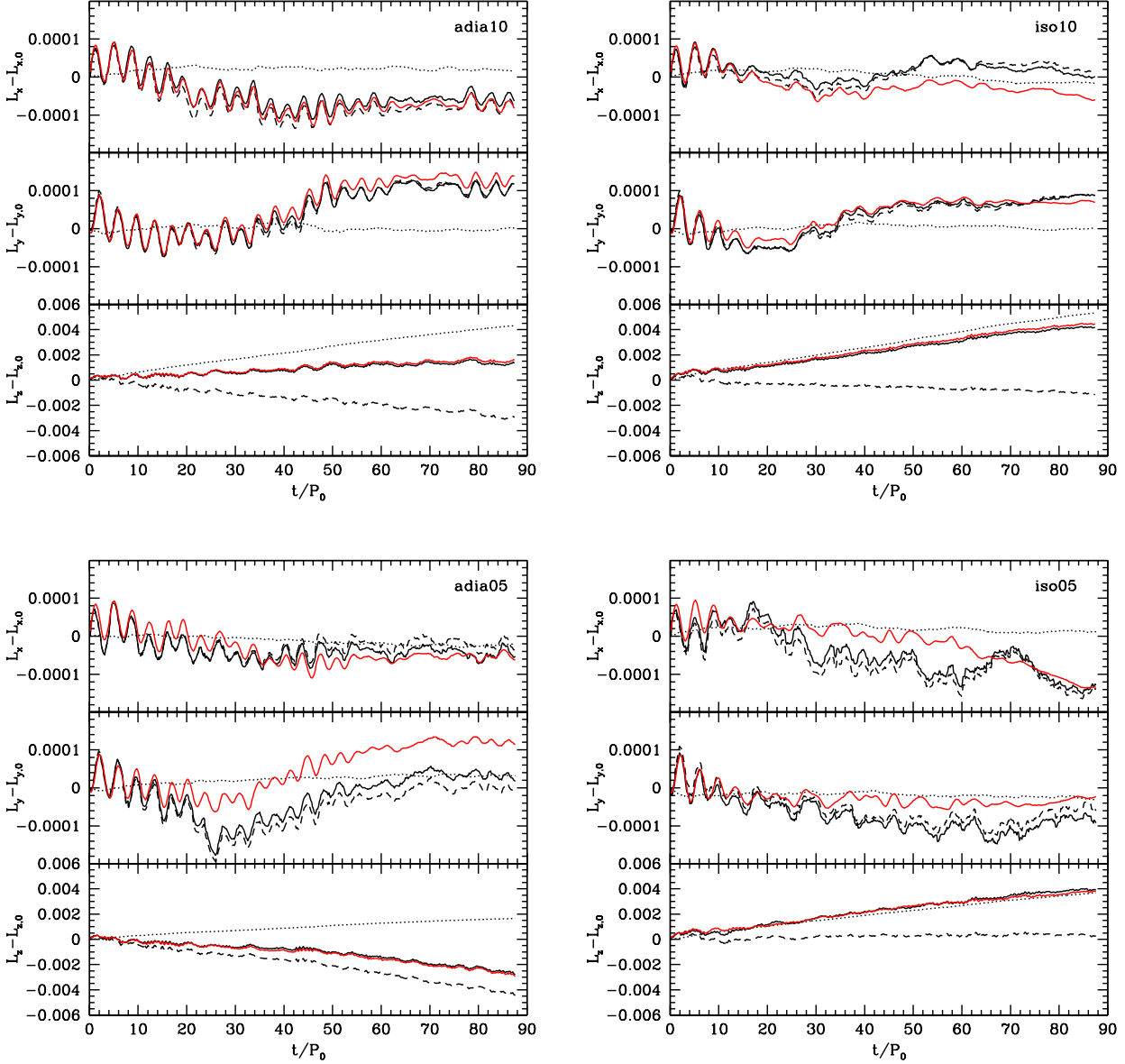
Figure 4. Consistency check of the evolution of the binary angular momentum components for all the simulations. In each plot, the L_x, L_y and L_z component evolution is shown from the top to the bottom. In each panel, the dashed line is the ΔL exchange balancing the gravity torques at each time step, the dotted line is the ΔL exchange computed from the accreted particles, and the solid black line is the sum of those two. For comparison, the red line is the angular momentum evolution taken directly from the raw simulation data. All ΔL are in units of $[M_0 a_0 V_{c,0}]$.

to the dominance of accretion in the angular momentum budget, and will be explained in § 3.2 below.

As a general rule, the accretion contribution to the binary **L** evolution (i.e., the accretion torque) is at least comparable to the effect of the gravitational torques. It is therefore also interesting to see the accretion contribution to the evolution of the binary orbital elements. Having stored all the accretion events, this can be done separately by simply evolving the binary from a_0 and e_0 only by adding one accreted particle after the other, imposing linear momentum conservation. This "*would-be*" evolution of $e(t)$ and $a(t)$, accounting only for the accretion effect, is shown in black in

all panels of Fig. 3. It is clear that $e(t)$ is mainly driven by gravitational torques, with accretion playing a negligible role. This is in line with our previous findings (Roedig et al. 2011), where the evolution of the eccentricity was attributed mainly to the gravitational interaction between the binary and the overdensities excited by its quadrupolar potential in the inner rim of the circumbinary disc. Conversely, the $a(t)$ plots highlight the importance of accretion for the semimajor axis evolution. In the *iso05* case, the binary shrinking due to accretion is actually larger than the total one, meaning that the disc torques would force the binary to expand; an effect similar to that described by Lin & Papaloizou (2011) in

the context of planetary migration in self-gravitating discs. Note that in the *adia* cases $\dot{a}$ is dominated by the effect of the disc. This explains the match between such simulations and the Ivanov et al. (1999) analytical model based on angular momentum transport through the disc (Cuadra et al. 2009).

3.2   Dissection of the binary evolution into its components

So far, we have separated the relative contribution of gravitational torques and accretion to the binary angular momentum budget. We now investigate how the angular momentum change is distributed among the relevant binary quantities. As clearly shown in Fig. 4, L_x and L_y show only small fluctuations (and therefore remain small compared to L_z, since the binary initially orbits in the x–y plane). From here on, we will therefore concentrate on the dominant L_z component. The binary angular momentum is

$$L_z = \mu\sqrt{GMa(1 - e^2)}, \tag{4}$$

where $\mu = M_1 M_2 / M$ is the binary reduced mass. Eq. (4) can be differentiated to separate the contribution of each single relevant quantity to the angular momentum change:

$$\frac{\dot{L}_z}{L_z} = \frac{\dot{a}}{2a} + \frac{\dot{M}}{2M} + \frac{\dot{\mu}}{\mu} - \frac{e}{1 - e^2}\dot{e}. \tag{5}$$

By directly measuring a, e, M, μ from the simulation, we can evaluate each single term and decompose the L_z evolution accordingly. This is shown in Fig. 5 for all the four runs. Note that the sum of the four contributions (solid black line in each panel) closely matches the measured L_z evolution directly measured from the simulation (red), validating our first-order expansion.

It is worth noting that the increase of L_z is perfectly compatible with semi-major axis shrinkage and eccentricity growth. In fact, Eq. (5) can be inverted to obtain

$$\frac{\dot{a}}{a} = \frac{2T_z}{L_z} - \frac{\dot{M}}{M} - \frac{2\dot{\mu}}{\mu} + \frac{2e}{1 - e^2}\dot{e}, \tag{6}$$

where we used the fact that $\dot{L}_z \equiv T_z$. Even if the total torque is positive, and the eccentricity grows, the binary can shrink because of the negative contribution of the M and the μ terms. In particular, as we will see below, the higher accretion onto the secondary hole results in a large increase of μ (long-dashed line in Fig. 5) which is the main driver of the binary angular momentum growth. Eqs. (5) and (6) highlight the importance of accretion in determining the binary temporal evolution.

4   GRAVITATIONAL TORQUES

As pointed out in the previous Section, understanding secular dynamics of BHBs in gaseous environments is closely tied to studying the interplay between long distance gravitational forces, hydrodynamics and accretion. In this Section, we focus on the torques coming from the self-gravitating gaseous disc, investigating the influence of regions at different distances from the BHB.
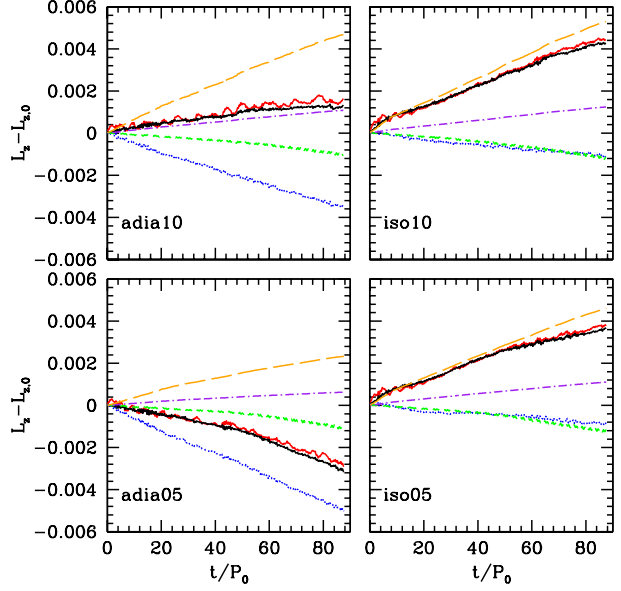

Figure 5. Decomposition of the L_z evolution for the four runs. The ΔL_z contributions stem from a (dotted), e (dashed), M (dot dashed) and μ (long dashed) variations separately. The sum of the four contributions is given by the solid black line, whereas the solid red line is, as in Fig. 4, the angular momentum evolution taken directly from the raw simulation data. All ΔL are in units of $[M_0 a_0 V_{c,0}]$.

4.1   Time averaged torque profiles

Gravitational torques exerted by the disc onto the BHB can be directly calculated at each snapshot from Eq. (2). It is of great interest to understand where such torques originate, and given the cylindrical nature of the problem, it is natural to investigate their azimuthally-averaged radial distribution. We take r to be the projected radial coordinate (in the x–y plane) from the binary CoM, and we define dT/dr to be the differential torque, integrated over the azimuthal coordinate and the disc height. The total average torque exerted by gas in the projected distance interval $[a, b]$ from the binary CoM is

$$\langle T_{[a,b]} \rangle = \left\langle \int_a^b \frac{dT}{dr} dr \right\rangle, \tag{7}$$

where $\langle \cdot \rangle$ denotes temporal averaging over the entire simulation.

In Fig. 6, we show the time averaged differential torque acting on the binary, $\langle dT/dr \rangle$ (blue), together with its integral according to Eq. (7) (black). We also decompose the former in the two components acting on the primary (green) and the secondary (red) BH. All torques are null at the binary corotation radius we therefore show the total torque by integrating from this point inwards ($\langle T_{[1,0]} \rangle$, binary region) and outwards ($\langle T_{[1,\infty]} \rangle$, disc region).

In all simulations, the local average torque shows an oscillatory behaviour with a sharp maximum at the location of the secondary BH, $r \sim 0.75$, and a deep minimum in the cavity region at $1 < r < 2$. In the body of the disc ($r > 2$) positive and negative peaks alternate, but they are shallow and almost cancel out, giving a negligible contribu-
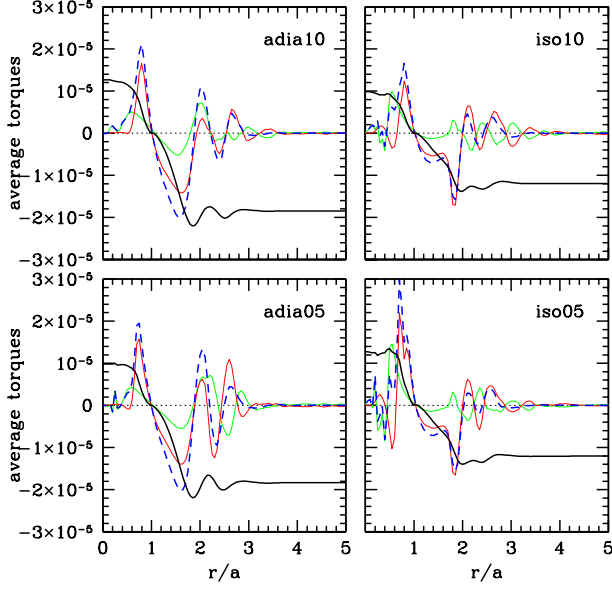
Figure 6. Differential torques dT/dr in units of $[GM_0^2 a_0^{-2}]$ averaged over the entire simulations. In each panel we show the differential torque on the primary (green), on the secondary (red), the sum of the two (blue), and the total integrated torque (black) according to Eq. 7. This latter is integrated starting from a inwards and outwards. Notably, the inward torque is positive, whereas the outward torque is negative.

tion to the total torque (as witnessed by the fact that the integrated torque is basically constant for $r > 2$). Note that the torque on the secondary BH is always larger than the torque on the primary, due to its proximity to the outer disc resulting in a stronger interaction. The general behaviour is qualitatively the same in the *adia* and *iso* runs. In this latter case, however, we found a much sharper negative peak at $r \approx 1.7$ followed by a smaller secondary negative bump at $r \approx 1.2$. This appears to be an artefact of the sudden change in EoS of the gas inside the cavity, at $r = 1.75$. The net result is a smaller negative $\langle T_{[1,\infty]} \rangle$ which has important consequences on the binary evolution. We see in fact that in the *iso* runs $\langle T_{[1,0]} \rangle$ and $\langle T_{[1,\infty]} \rangle$ almost cancel out, meaning that, overall, gravitational torques do not change the binary angular momentum. Conversely, in the *adia* runs $\langle T_{[1,0]} \rangle$ is much smaller (in absolute value) than $\langle T_{[1,\infty]} \rangle$, implying an efficient angular momentum transfer from the binary to the gas (MM08; Cuadra et al. 2009).

4.2 Spectral analysis

We now consider the torque evolution in time. We separately discuss torques coming from different disc regions by showing both the time series and their associated power spectra. We cut the spatial domain into the following radial annuli:

   (i) $0 \; a < r < 10 \; a$: the entire domain
   (ii) $0 \; a < r < 1 \;\; a$: the 'binary region'
   (iii) $1 \; a < r < 1.8a$: the 'cavity region'
   (iv) $1.8a < r < 2.5a$: the 'rim region'
   (v) $2.5a < r < 10 \; a$: the 'disc region'

The associated time series and power spectra are shown respectively in the left and right panels of Fig. 7.

In all the simulations, the overall torque (i), shows a clear periodic oscillation, much larger in amplitude than its average value. The power spectrum unveils several distinctive peaks, with relative amplitudes that can vary significantly for different simulations. In particular, peaks in the *iso* simulations are much sharper and better defined. This is because in the *adia* simulations the BHB shrinks significantly, resulting in a broadening of the characteristic frequencies. Moreover, as we shall see in the next section, the disc sub-structures are much better defined in the *iso* runs, giving rise to neater features.

In the binary region (ii) the torque is mostly coherent and positive. Because the torque strength in (ii) is regulated by the mass inflow, it shows periodicities that are related to the accretion flow: a disc component around $f \approx 0.25 P_0^{-1}$ (corresponding to the disc peak density at $r \approx 2.5a$), the forcing frequency of the binary at $f = P_0^{-1}$, and the beat between these two at $f \approx 0.75 P_0^{-1}$ (see Section 5 and Roedig et al. (2011) § 5.1). In the cavity region (iii) the torque is negative on average but strongly oscillating. Several periodicities are detectable, the most striking being a peak at $f \approx P_0^{-1}$ which appears again to be directly related to the binary period. In the rim region (iv) the torque is highly oscillating, and the strongest feature is a sharp peak at $f \approx 1.3 P_0^{-1}$, whereas in the disc region (v) the only significant spectral component is at $f \approx 1.7 P_0^{-1}$. As a general trend, moving from the inner region to the disc body, torques become incoherent (i.e. they average to zero) and strongly oscillating (compare the power spectra scales in the different panels of each plot).

4.3 Interpretation: torque origin and location in the disc

In this Section, we provide a global interpretation of the features observed both in the radial distribution of the time averaged torques and in their temporal evolution. The arguments discussed below are supported by Figs. 8–9–10 and by Tab. 2.

4.3.1 Origin of the positive and negative peaks

It seems natural to compare the torque radial profiles obtained by our simulations with linear theory perturbation, in which torque minima and maxima are connected to outer Lindblad resonances (OLRs). It is in fact tempting to associate the torque minimum at $r \approx 1.6a$ with the 2:1 OLR. We should however be careful in pushing this interpretation too far, since, as already pointed out by MM08 and S11, the assumptions of linear theory are not satisfied in this context. Most importantly, looking at the upper panels of Figs. 8 and 9, we notice that the region $r < 2a$ is almost devoid of gas, and the streams are almost radial. Mass fluxes reported in Tab. 2 clearly show that, at any radius, there are always fluxes of ingoing and outgoing mass, resulting in a steady net inward flux consistent with the accretion rate onto the two BHs. A strict OLR interpretation of the torque minimum at $r \approx 1.6a$ would instead require particles in circular orbit at that radius, experiencing a secular effect due
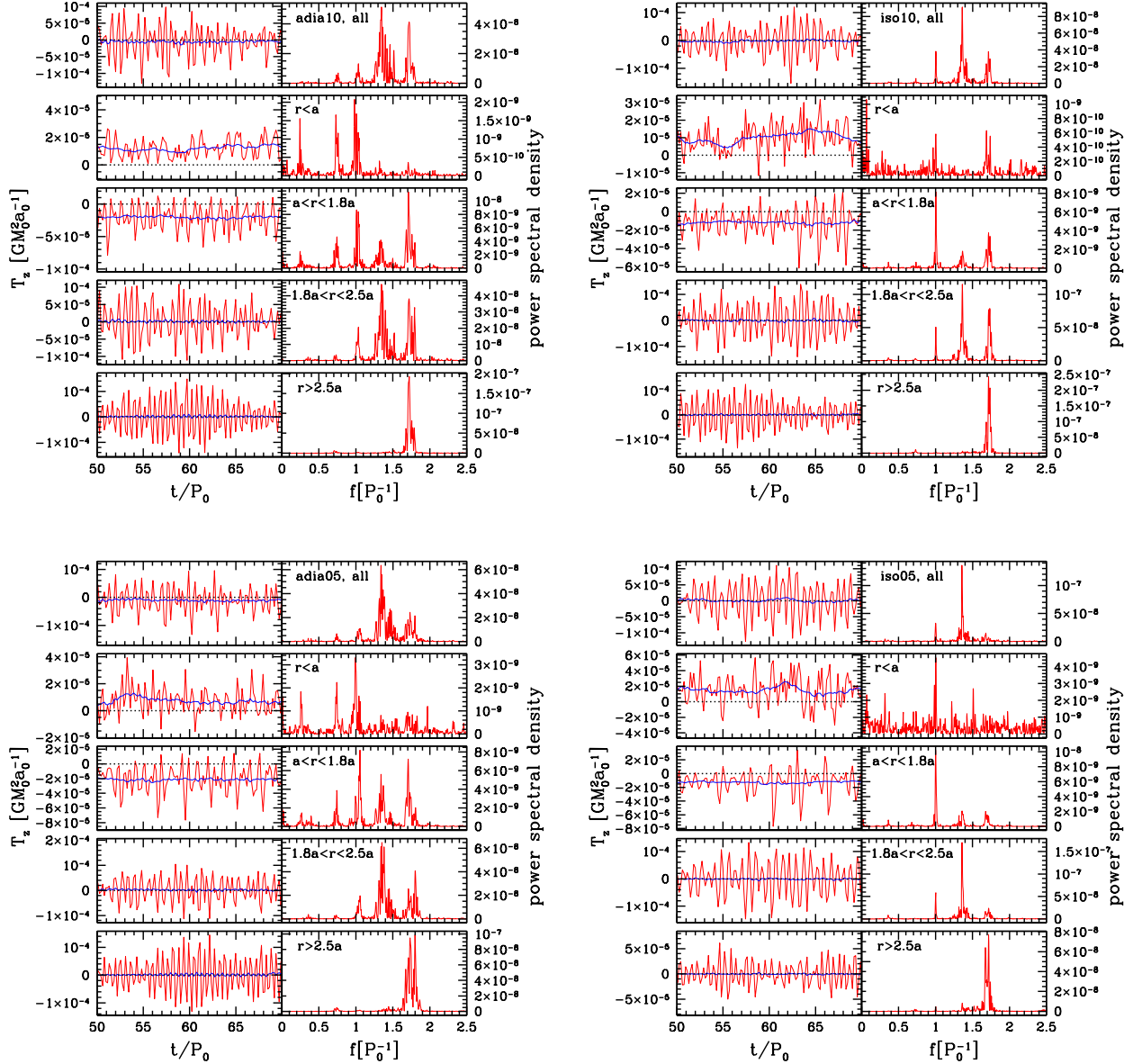
Figure 7. Each plot depicts the torques exerted by the disc on the BHB in the time domain (left panels) and in the frequency domain (right panels). In each plot, from the top to the bottom, pairs of panels refer to the five domains discussed in the text: total torque (i), torque exerted by the material located at $r < a$ (ii), $a < r < 1.8a$ (iii), $1.8a < r < 2.5a$ (iv) and $r > 2.5a$ (v). In each left panel, the red line is the raw oscillating torque, and the blue one is the torque smoothed over three periods to show the average behaviour. In the associated right panel, we plot the power spectrum as a function of frequency in units of the initial binary orbital frequency. All torques strongly oscillate, showing several characteristic frequencies, however, note the different scales of the panels.

to the phase-coherent periodic forcing of the binary; this is not what happens within the cavity region. The strongest 2:1 OLR is certainly responsible for the evacuation of the gas close to the binary and for the formation and mainte-nance of a cavity, however cannot be directly responsible for the coherent torque seen in the cavity region. This is also supported by the fact that MM08 and S11 find a minimum at the same location ($r \approx 1.6 - 1.7a$) for an equal mass binary, where the 2:1 resonance is absent (because of the symmetry of the forcing potential), and the location of the strongest OLR (3:2) would be at $r \approx 1.3a$. The strong neg-

ative torque in the cavity region has a purely kinetic origin: material ripped off the disc edge forms well defined streams *following* the two BHs, which are clearly distinguishable in both the surface density plots shown in Fig. 8 and 9. The streams are responsible for the yellow tails following the two BHs at $\sim 1.5a$ in the torque density panels, which lead to a net negative torque. Conversely, at $r \gtrsim 2a$, we have a well defined, almost circular disc, and the torque density peaks at $r \approx 2a$ and $r \approx 2.5a$ can be identified with the loci of the strong 3:1 and 4:1 OLRs (Artymowicz & Lubow 1994).

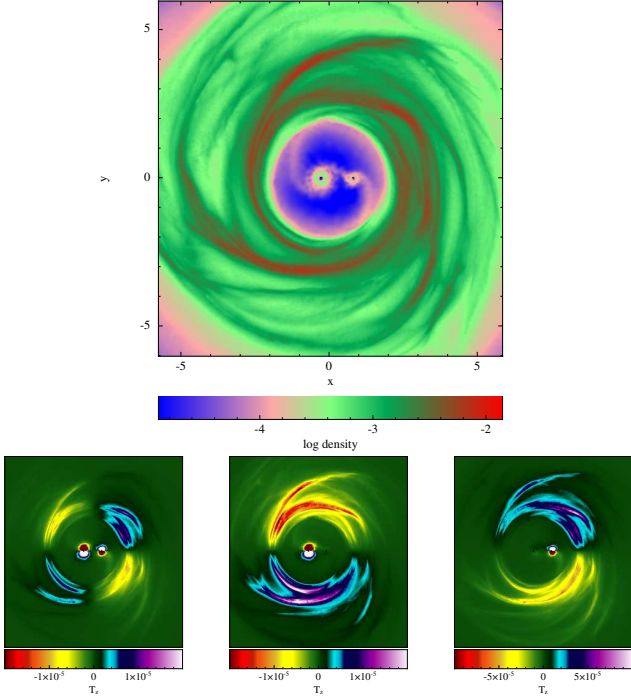Our simulations also allow us to investigate the torques

Figure 8. Top panel: typical instantaneous logarithmic surface mass density of the *iso05* simulation. Bottom row: combined surface torque density exerted by the disc onto the binary (left panel), onto the primary BH (central panel) and onto the secondary BH (right panel). All plots are in code units: $G = M_0 = a_0 = 1$.
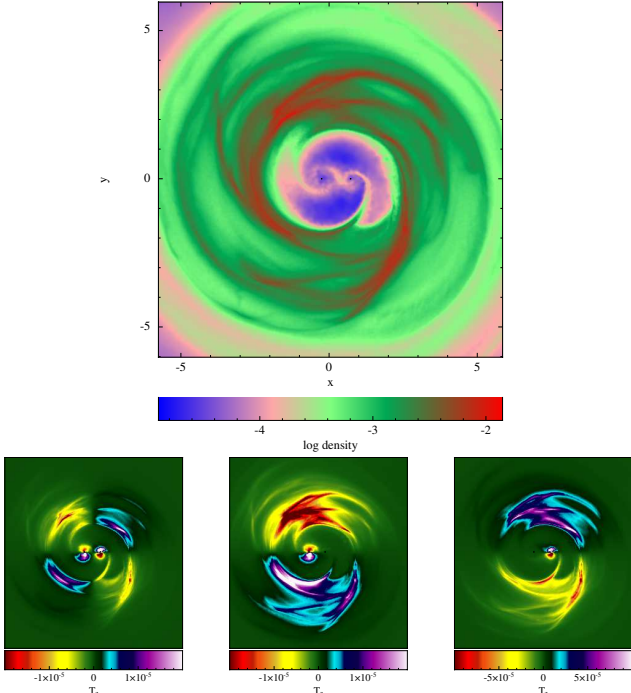

Figure 9. Same as Fig. 8 but for the *adia05* run. Here the features highlighted above are even more evident (especially the symmetric overdensities at the inner edge of the disc).
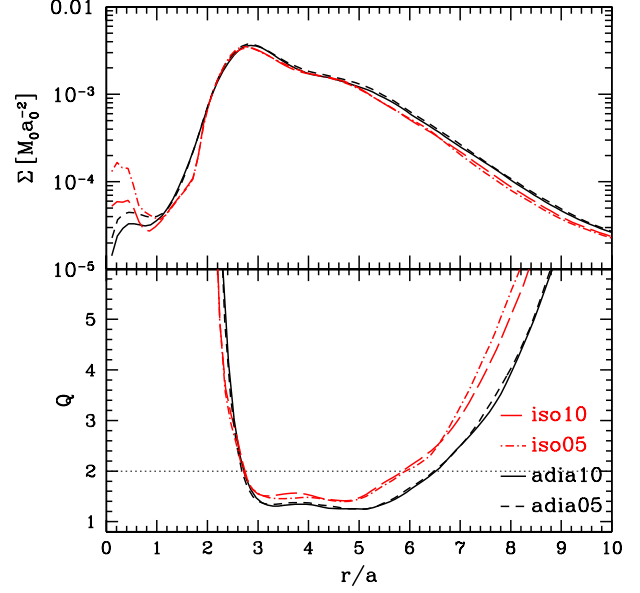

Figure 10. Disc properties: average surface density (top panel), and Toomre parameter Q (bottom panel) as a function of r. Line style denotes iso10 (long dashed), iso05 (dot dashed), adia10 (solid) and adia05 (dashed).

within the binary corotation radius at $r < a$, a region often excised in grid-based simulations (see MM08 and S11). Here we find strong positive torques on both BHs. This is because the infalling material approaches the BHs at super-Keplerian velocities, and bends in a horseshoe fashion, exerting a net positive torque in front of them. In fact, the maximum positive torque basically coincides with the location of the two BHs (sharp peak at $r \approx 0.75a$ for the secondary and a broader peak around $r \approx 0.3a$ for the primary, see Fig. 6). The very same effect, in the context of planetary migration, was discussed by Lin & Papaloizou (2011).[7] Note that the positive torque is related to this 'stream bending', and not directly to the small discs of gas orbiting each BH; its magnitude is in fact similar in the *iso* and in the *adia* simulations, even though in the former, the mass in the minidiscs is significantly larger as shown by the time and azimuthally averaged surface density profiles in the upper panel of Fig. 10.

4.3.2 Disc structure and characteristic torque frequencies

The surface density profiles in Fig. 8 and 9 highlight some clear differences between the *iso* and the *adia* runs: (i) the appearance and shape of the minidiscs; (ii) the amount of gas feeding the streams; (iii) the definition of the inner disc edge. In the *iso* runs, we find a large amount of gas forming mini-discs around both BHs and an almost empty cavity except for two tenuous streams connecting the outer edge

[7] Lin & Papaloizou (2011) found that such positive torque can in principle counter-balance the negative torque due to the disc and the tails, causing, in their case, angular momentum to be transferred *to* the planet, resulting in an *outwards* migration.

Table 2. Accretion rates onto the binary and mass fluxes F in units $M/P_0 \times 10^{-5}$ at two selected distances to the binary CoM: $r_1 = a$ and $r_2 = 1.5\,a$. $\dot{M_1}$ and $\dot{M_2}$ are the average accretion rates on M_1 and M_2 respectively, while $\dot{M}$ is the sum of the two. At both selected distances, F_{in} and F_{out} represent the ingoing and outgoing fluxes, and $F_{\text{net}} = F_{\text{in}} - F_{\text{out}}$ is the net ingoing flux. All quantities have been averaged over 90 binary orbits.

					$r_1 = a$			$r_2 = 1.5a$	
Model	$\dot{M_1}$	$\dot{M_2}$	$\dot{M}$	F_{in_1}	F_{out_1}	F_{net_1}	F_{in_2}	F_{out_2}	F_{net_2}
iso10	4.5	10.7	15.2	19.6	4.5	15.1	33.7	18.8	14.9
iso05	4.2	9.2	13.4	19.1	5.5	13.6	31.7	18.4	13.4
adia10	3.8	9.5	13.3	17.6	4.3	13.3	42.8	29.7	13.2
adia05	3.2	4.6	7.8	13.5	5.8	7.7	36.0	28.4	7.6

to the mini-discs. The edge of the disc is quite circular and well defined. Conversely, due to the gas inside the cavity being hotter in the *adia* runs, the streaming activity is more violent with thick spirals that do not settle into well defined mini-discs, but rather form a diluted, ∞-shaped cloud around the binary. The edge of the disc is strongly disturbed by the ripped out streams and is usually not circular. The different streaming activity is also confirmed by numbers in Tab. 2, where we collect the average inwards and outwards mass fluxes at $r = 1.5a$ and $r = a$. Mass fluxes are generally larger in the *adia* case. Note that this does not necessarily result in larger accretion, as outgoing fluxes are also larger in this case. Most of the material in the streams, does not end up in an accretion flow, but is accelerated back to the disc (a sort of 'slingshot') impacting on the inner edge, an effect already seen and extensively described by MM08 and S11. The amount of impacting gas is 50% larger in the *adia* case, possibly contributing to the inner edge destabilization and to the larger perturbation in the disc structure. The appearance of spirals in the disc is related to the behaviour of the Toomre Q parameter, shown in the bottom panel of Fig. 10, which quantifies the degree of self-gravity of a disc. Not surprisingly the disc develops a spiral pattern in the region $3a \lesssim r \lesssim 5a$, where, in fact, we find that the Toomre parameter reaches its minimum value $Q \approx 1.5$ (Cuadra et al. 2009). The shape of the spiral arms varies much in time, and their definition is different from simulation to simulation. However, at any time we find spiral structures with 2, 3 or 4 arms, which remain confined between $3a < r < 5a$.

The disc structures highlighted above are reflected in the torques depicted in the lower panels of Fig. 8 and 9. The total torque shows a typical quadrupolar structure, which leads to rapid oscillations averaging to zero in the disc body. Conversely, as already discussed, in the inner cavity we can appreciate the yellow tails following the two BHs at$\sim 1.5a$, leading to a net negative torque.

The main peaks observed in the torque power spectra must therefore arise from the structures we just described. In particular we identified the overdensities at $r \approx 2a$ in the inner rim of the disc, and the spiral structures at $r \gtrsim 3a$ in the main body of the disc. The main torque frequencies must come from the interaction between the forcing binary quadrupolar potential and such overdensities propagating in the disc. To test this hypothesis, we mimic the situation by placing test particles in circular orbits at $r = 2a$ and $r = 3.5a$ around a circular binary. We compute the torques and
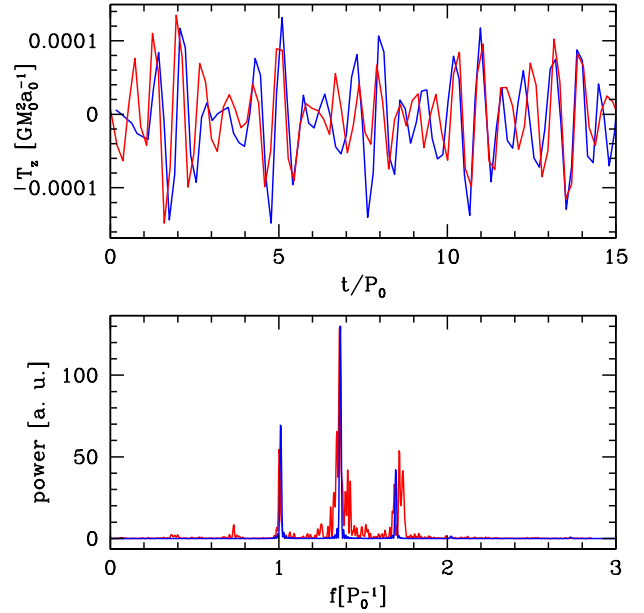

Figure 11. Simple test model for the periodicity generated in the outside disc, i.e. at $r > a$. In the top panel we show the temporal evolution of the torque, whereas in the bottom panel we show the Fourier transform. In each panel, the blue curve is obtained by placing three point masses at distance $1.6a$, $2.1a$, $3.5a$ from a circular binary, and the the red is the torque found in the *iso10* simulation.

show them as blue lines in Fig. 11. The natural frequency between a quadrupolar potential oscillating with frequency f_1 and an overdensity orbiting at frequency f_2 is the beat frequency $2f_1 - f_2$, and this is what we see in the Fourier spectrum. The beats between the binary and the particles at $r = 2a$ and at $r = 3.5a$ give rise to sharp peaks seen at $f \approx 1.35P_0^{-1}$ and $f \approx 1.7P_0^{-1}$, respectively. The fact that such peaks are much sharper in the *iso* simulations stems from two facts: (i) the binary does not significantly shrink in the *iso* runs, limiting the broadening of the spectral feature and (ii) the disc features (disc edge and spiral arms) are much more defined in this case, and the torques are well localized. This can be also seen by comparing the much neater torque structure in the bottom panel of Fig. 8 to the blurry one of Fig. 9. The $f \approx P_0^{-1}$ peak of the blue line in Fig. 11 is obtained by placing a third particle at $r =$

1.6a, a separation corresponding to the maximum negative torque inside the cavity. However, Fig. 7 shows that the peak at $f \approx P_0^{-1}$ is stronger at $r > 1.8a$ than in the $a < r < 1.8a$ region, meaning that it must be mostly directly related to the periodicity at which the binary rips gas off the disc edge (i.e. the binary period), and not to a specific radius in the cavity. Finally, as already noticed, torques in the binary region are related to the mass fuelling the two BHs, and therefore show periodicities related to the binary ($f = P_0^{-1}$), to the inner rim of the disc ($f \approx 0.25 P_0^{-1}$) and to the beat between the two ($f \approx 0.75 P_0^{-1}$). Note that the latter two are much more evident in the *adia* runs, where the disc rim overdensities feeding the accretion streams are more pronounced.

5 ACCRETION

In Tab. 2 we also show the average mass accretion rates. We recall here that a particle is considered accreted when it crosses the sink radius of one of the BHs. Then both its mass and its linear momentum are added to the BH, ensuring the global conservation of both quantities. The mass accretion rate is almost independent on the sink radius in the *iso* simulation, where instreaming gas settles in well defined accretion discs progressively loosing angular momentum. Conversely, in the *adia* case, the accretion rate scales almost linearly with the sink radius, suggesting a direct relation to the BH cross section (defined by the sink radius itself).

It is particularly interesting to compare the accretion rate to the mass flow rates. Firstly we notice that in all simulations the accretion rate and the mass flow rates at $r = a$ and $r = 1.5a$ are nearly the same, meaning that the system is in a steady state configuration. Interestingly, the mass accretion rate is $\sim 25\%$ lower than the inflow rate at $r = a$. This means that not all the material crossing $r = a$ is accreted, an assumption commonly adopted in grid simulations where the $r < a$ region in excised. Part of the gas suffers a slingshot impacting back to the disc, affecting further the disc–binary angular momentum transfer.

In the top panel of Fig. 12 we show the temporal evolution of the accretion rate on the primary hole, $\dot{M}_1$, on the secondary hole, $\dot{M}_2$, and the sum of the two, $\dot{M}$. As already found in Cuadra et al. (2009); Roedig et al. (2011), $\dot{M}_2$ is a factor ~ 2 larger than $\dot{M}_1$, due to the closer interaction between the secondary BH and the disc. The relative mass growth $\delta M/M$ is therefore about six time faster for the secondary BH, implying the binary mass ratio will tend toward $q \approx 1$ if this condition persists over the entire evolution of the system. Accretion rates are strongly modulated in time, and notably, $\dot{M}_2$ shows a striking periodicity related to the binary orbital period, whereas $\dot{M}_1$ is dominated by longer timescale fluctuation, related to the overdensities developing at the inner rim of the circumbinary disc.

The Fourier transform of $\dot{M}$ is given in the lower panel of Fig. 12. We observe the usual three distinctive peaks observed in the torques coming from the binary region, as shown by the central panel of the figure. It is clear that the accretion and inner-torque periodicities are intimately connected, both reflecting the temporal evolution of the mass inflow in the binary region (ii).
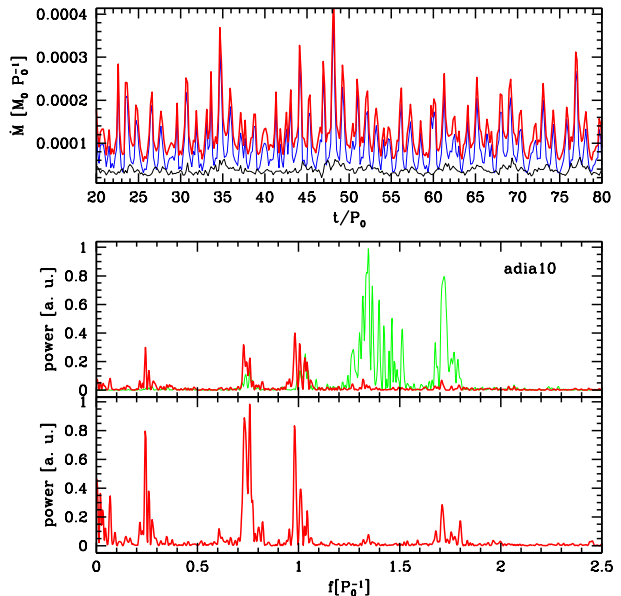

Figure 12. Accretion onto the two BHs. Top box: accretion rate as a function of time. The red line is the total accretion rate while the blue and black lines are the accretion rates onto the secondary and the primary respectively. Lower box: Fourier transform of the total accretion rate (lower panel) and of the torques (upper panel). In the upper panel, the green line is the total torque (highest peak normalized to 1) and the red line is the torque exerted by the material at $r < a$ (multiplied by ten).

Finally we can check the orientation of the angular momentum vector of the accreted material in the reference frame of the accreting BH. This number quantifies the level of 'coherence' of the accretion flow, and has important consequences for the individual BH spin evolution and the magnitude of gravitational recoil at the coalescence (Bogdanović et al. 2007; Dotti et al. 2010; Kesden et al. 2010; Volonteri et al. 2010; Lousto & Zlochower 2011; Lousto et al. 2012). At each snapshot we therefore compute the average L_z and $\mathbf{L}$ of the accreted particles *in the accreting BH reference frame*, and the angle $\theta = \arccos(L_z/\mathbf{L})$ defining the degree of misalignment with respect to the z axis. Our results are similar to what already found by Dotti et al. (2009), although in the cited study the spin evolution was studied only before the gas scouring. More specifically, an isothermal EoS leads to extremely coherent accretion flows, with fluctuations in the angular momentum direction of the mini-discs of few degrees. In the adiabatic case, the orientation of the minidisc orbiting the secondary changes by at most ≈ 20 degrees, and has an average excursion of 7 degrees, 50% bigger than the oscillations in the primary disc. Assuming that the BH spins have efficiently aligned with the circumbinary disc before the opening of the cavity (Dotti et al. 2010) this implies that the efficient spin-up of the binary will continue following cavity opening.

6   COMPARISON WITH PREVIOUS WORKS

The binary evolution and torque structure have been previously investigated by MM08 and S11, as described in the introduction. In particular, we can compare results regarding the average gravitational torques and the mass accretion rates. While both of them can be expressed in several ways, we find it practical to normalize these quantities to the disc mass, M_d, initial binary period, P_0, and initial binary angular momentum magnitude, L_0. In these units we can write:

$$\langle T_{[1,\infty]} \rangle = \Gamma_1 L_0 M_d P_0^{-1} \qquad (8)$$

$$\dot{M} = \Gamma_2 M_d P_0^{-1} \qquad (9)$$

Here $M_d = \pi \Sigma_{\rm p} r_{\rm p}^2$ is the disc mass computed using the peak surface density[8] $\Sigma_{\rm p}$. In both MM08 and S11, $r_{\rm p} \approx 3a$, close to what we find in our discs (see Fig. 10). Before proceeding with this comparison we should mention several issues that has to be considered. Firstly $L_0 = (M_0/4)(GM_0 a_0)^{1/2}$ for the circular equal mass binary simulated by MM08 and S11, whereas in our simulation with $q = 1/3$ we have $L_0 = (3M_0/16)(GM_0 a_0)^{1/2}$ (assuming a circular binary). Secondly, the concept of 'accretion rate' is somewhat ill defined in grid based simulation with an excised central region. The inner boundary of the calculation is at $r = a$ for MM08 and $r = 0.8a$ for S11, and in both cases, whatever crosses that boundary is considered accreted. As already discussed (see Tab. 2) $\approx 25\%$ of the mass crossing $r = a$ is accelerated back to the disc edge extracting angular momentum from the binary (an effect already seen and described extensively by MM08 and S11 for the material inflowing in the cavity but not reaching the excised region). We can therefore consider MM08 and S11 to overestimate the accretion rate by a factor of 25%. Lastly, MM08 and S11 can compute gravitational torques only for $r \gtrsim a$, outside the binary corotation radius[9]. As shown by both studies (and independently recovered by us), gravitational torques *exerted by the disc elements on the binary* are negative in this region.

For the sake of the comparison we use the *iso05* and the *adia05* runs. In the torque computation, we find $\Gamma_1 = -3.5 \times 10^{-3}$ for the former and $\Gamma_1 = -5.3 \times 10^{-3}$ for the latter. This can be compared to -1.26×10^{-3} of MM08 and -1.8×10^{-2} of S11. Our gravity torques are a factor 3–4 larger than MM08 and a factor 4–5 smaller than S11. Concerning the accretion, we get $\Gamma_2 = 1.1 \times 10^{-3}$ for the *iso05* run and $\Gamma_2 = 6 \times 10^{-4}$ for the *adia05* run, to be compared to $\Gamma_2 = 1.2 \times 10^{-4}$ of MM08 and $\Gamma_2 = 6 \times 10^{-3}$ for S11. Our accretion rates are a factor 5–10 larger than MM08 and a factor 5–10 smaller than S11. The similar scaling between $\langle T_{[1,\infty]} \rangle$ and $\dot{M}$ is not surprising, since, as discussed in Section 4, the former is directly linked to the streams fuelling the BHs.

7   DISCUSSION AND CONCLUSION

The evolution of BHBs in circumbinary discs remains largely an open issue. Here we carried out a detailed study of the torques acting on the BHB, including the effect of the outer disc, the mass flowing in the cavity and, for the first time, of the gas entering the BHB region and eventually accreting onto the two BHs. We paid particular attention to investigating the individual contribution of different disc regions and we aimed at separating the effect of accretion from the effect of gravitational torques. The emerging picture is far more complex than the often adopted simple assumption that resonant torques arising at the disc inner edge transfer angular momentum from the BHB to the disc, causing the orbital decay (e.g. Papaloizou & Pringle 1977; Goldreich & Tremaine 1980; Ivanov et al. 1999; Armitage & Natarajan 2002; Haiman et al. 2009).

Firstly, as already pointed out by a number of authors (e.g. MM08, S11), the presence of a BHB clearing a cavity in the disc *does not* prevent gas inflows and eventual accretion onto the two BHs. Such inflowing gas has a non negligible role in defining the BHB–disc mutual evolution; it forms streams that follow the BHs, eventually exerting a net *negative* torque in the cavity region. The inflows catch-up with the BHs at a super-Keplerian speed, bend in front of them, thus exerting a net *positive* torque inside the binary corotation radius (i.e. at $r < a$). We therefore conclude that the origin of the dominating gravitational torques on the binary is purely kinematic, and can be understood without directly invoking resonances of the forcing binary potential with the disc.

The strong positive gravitational torque is related to the gas inflows only, and not to the formation of minidiscs around the two BHs nor to the eventual accretion. This becomes clear by inspecting Figs. 6, 10 and Tab. 2; although there is a factor up to ten difference in the mass bound to the BHs in minidiscs, and a factor of three difference in the accretion rate among the simulations, the positive torque is almost the same. This is because the gravitational torque is only related to the *inflowing* mass bending in front of the BHs, which is of the same order in all simulations. Note that different thermodynamics lead to different negative/positive torque balance. Although this might be an artefact of the sudden change of EoS in the *iso* simulations, such a balance has to be better understood in order to assess the fate of the binary.

Torques exerted by gas in the main body of the disc ($r > 2a$) are instead negligible for the long term evolution of the system, since they average to zero (Fig. 6)[10]. Local torque maxima can be associated to the 3:1 and 4:1 OLRs (Artymowicz & Lubow 1994). Given the nature of the forcing potential, a quadrupolar torque pattern naturally develops (Figs. 8 and 9) causing a time oscillating torque (Fig. 7) with characteristic frequencies related to the beat between twice the binary frequency and the characteristic orbital frequencies of inhomogeneities developing in the disc in form of inner edge overdensities and spiral arms (Fig. 11).

Accretion plays an important role in the binary angular momentum budget. The binary can actually gain angular momentum even if it shrinks and its eccentricity increases. This is because accretion deposits a significant amount of angular momentum in the system by increasing its mass and

---

[8] Note that we have a physical disc mass in our simulations, but we use this quantity to ease the comparison with MM08 and S11.
[9] S11 already pointed out the change of sign of the torques at $r = a$.

[10] Note that this region excludes the disc edge

mass ratio (see Eq. (5)). The peculiar case of *iso05* is quite interesting: here the total gravitational torque exerted by the gas is almost null (Fig. 6). However, the BHB–disc mutual torques are responsible for the eccentricity growth, meaning that, if angular momentum was transferred by gravitational torques only, the BHB would be forced to expand. This is what we see in the upper-right panel of Fig. 3, where we show that the accretion-driven shrinking is faster than the actual evolution found in the simulation. In this case, gravitational torques alone would force the BHB to *expand*, whereas accretion is responsible for the shrinkage. Although whether this happens in Nature is questionable, it highlights the complexity of the BHB–disc interplay.

We should, nonetheless, be careful in drawing any conclusion about accretion from our simulations. If we scale our system to the fiducial binary of Roedig et al. (2011) and set $M_1 = 2.6 \times 10^6 \, \mathrm{M_\odot}$ and $a_0 = 0.039$ pc, then the accretion rate we find corresponds to about 20–40$\dot{M}_{\rm Edd}$ for the secondary BH, and 4–7$\dot{M}_{\rm Edd}$ for the primary BH. In such situation, it is likely that most of the gas which is *numerically* accreted in our simulations will be expelled through outflows and winds. In this case, if the gas binds to the BHs before being expelled, it transfers its linear (and angular) momentum to the holes, even if not accreted (Nixon et al. 2011). However, its mass does not add-up to the binary, making the question of angular momentum transfer more delicate and worthy of deeper and more refined investigations.

The relatively low computational cost of our simulations allowed us to investigate different EoSs and sink radii $r_{\rm sink}$. The numerical size of $r_{\rm sink}$ has a minor impact on the general behaviour of the system, affecting the mass bound to the BH in minidiscs and the accretion rate in the *adia* case. Conversely, the adopted EoS has a major impact on the results. In the *iso* runs, tenuous streams leak from an almost circular disc edge and fuel two well defined minidiscs, whereas streaming activity is more violent in the *adia* case, with thick spirals leaking from a deeply distorted disc edge, forming a diluted, ∞-shaped cloud around the binary. This difference in streaming activity affects both the overall structure of the outer disc and the long-term binary evolution (as mentioned above). Although the extrapolation of the results of all our four simulations would imply a fast BHB coalescence (in less than 10^7 yr, for the fiducial binary parameters considered above), the almost perfect cancellation of the net gravitational torque in the *iso* simulations suggest that more realistic models for gas thermodynamics will be necessary to make clear-cut statements on this issue.

REFERENCES

Armitage P. J., Natarajan P., 2002, Astrophys. J. Lett., 567, L9

Armitage P. J., Natarajan P., 2005, Astrophysical Journal, 634, 921

Artymowicz P., Lubow S. H., 1994, Astrophys. J., 421, 651

Bate M. R., Bonnell I. A., 1997, Mon. Not. R. Astron. Soc., 285, 33

Bate M. R., Bonnell I. A., Price N. M., 1995, Mon. Not. Roy. Astr. Soc., 277, 362

Begelman M. C., Blandford R. D., Rees M. J., 1980, Nature, 287, 307

Bogdanović T., Reynolds C. S., Miller M. C., 2007, ApJ, 661, L147

Bryden G., Chen X., Lin D. N. C., Nelson R. P., Papaloizou J. C. B., 1999, Astrophys. J., 514, 344

Cuadra J., Armitage P. J., Alexander R. D., Begelman M. C., 2009, Mon. Not. Roy. Astr. Soc., 393, 1423

Cuadra J., Nayakshin S., Springel V., Di Matteo T., 2006, Mon. Not. R. Astron. Soc., 366, 358

Davies R. I., Tacconi L. J., Genzel R., 2004a, Astrophysical Journal, 613, 781

Davies R. I., Tacconi L. J., Genzel R., 2004b, Astrophysical Journal, 602, 148

Dotti M., Colpi M., Haardt F., Mayer L., 2007, Mon. Not. Roy. Astr. Soc., 379, 956

Dotti M., Ruszkowski M., Paredi L., Colpi M., Volonteri M., Haardt F., 2009, Mon. Not. Roy. Astr. Soc., 396, 1640

Dotti M., Sesana A., Decarli R., 2012, Advances in Astronomy, 2012

Dotti M., Volonteri M., Perego A., Colpi M., Ruszkowski M., Haardt F., 2010, Mon. Not. R. Astron. Soc., 402, 682

Downes D., Solomon P. M., 1998, Astrophysical Journal, 507, 615

Dutrey A., Guilloteau S., Simon M., 1994, Astronomy & Astrophysics, 286, 149

Escala A., Larson R. B., Coppi P. S., Mardones D., 2005, Astrophysical Journal, 630, 152

Fabbiano G., Wang J., Elvis M., Risaliti G., 2011, Nature, 477, 431

Foreman G., Volonteri M., Dotti M., 2009, Astrophysical Journal, 693, 1554

Gammie C. F., 2001, Astrophys. J., 553, 174

Goldreich P., Tremaine S., 1980, Astrophysical Journal, 241, 425

Greve T. R., Papadopoulos P. P., Gao Y., Radford S. J. E., 2009, Astrophysical Journal, 692, 1432

Gültekin K., Richstone D. O., Gebhardt K., Lauer T. R., Tremaine S., Aller M. C., Bender R., Dressler A., Faber S. M., Filippenko A. V., Green R., Ho L. C., Kormendy J., Magorrian J., Pinkney J., Siopis C., 2009, Astrophysical Journal, 698, 198

Günther R., Kley W., 2002, Astron. & Astrophys., 387, 550

Günther R., Schäfer C., Kley W., 2004, Astron. & Astrophys., 423, 559

Haiman Z., Kocsis B., Menou K., 2009, Astrophysical Journal, 700, 1952

Hayasaki K., 2009, Publications of the Astronomical Society of Japan, 61, 65

Hayasaki K., Mineshige S., Ho L. C., 2008, Astrophys. J., 682, 1134

Hayasaki K., Mineshige S., Sudou H., 2007, Publications of the Astronomical Society of Japan, 59, 427

Hennawi J. F., Strauss M. A., Oguri M., Inada N., Richards G. T., Pindor B., Schneider D. P., Becker R. H., Gregg M. D., Hall P. B., Johnston D. E., Fan X., Burles S., Schlegel D. J., Gunn J. E., Lupton R. H., Bahcall N. A., Brunner R. J., Brinkmann J., 2006, Astronomical Journal, 131, 1

Ivanov P. B., Papaloizou J. C. B., Polnarev A. G., 1999, Mon. Not. R. Astron. Soc., 307, 79

Kesden M., Sperhake U., Berti E., 2010, Astrophysical Journal, 715, 1006

Khan F. M., Just A., Merritt D., 2011, Astrophys. J., 732, 89

Komossa S., Burwitz V., Hasinger G., Predehl P., Kaastra J. S., Ikebe Y., 2003, Astrophys. J., 582, L15

Lin D. N. C., Papaloizou J., 1986, Astrophys. J., 309, 846

Lin M.-K., Papaloizou J., 2011, ArXiv e-prints

Lodato G., Nayakshin S., King A. R., Pringle J. E., 2009, Mon. Not. R. Astron. Soc., 398, 1392

Lousto C. O., Zlochower Y., 2011, Physical Review Letters, 107, 231102

Lousto C. O., Zlochower Y., Dotti M., Volonteri M., 2012, ArXiv e-prints

Lubow S. H., Seibert M., Artymowicz P., 1999, Astrophys. J., 526, 1001

MacFadyen A. I., Milosavljević M., 2008, Astrophys. J., 672, 83

Mayer L., Kazantzidis S., Madau P., Colpi M., Quinn T., Wadsley J., 2007, Science, 316, 1874

Mihos J. C., Hernquist L., 1996, Astrophysical Journal, 464, 641

Myers A. D., Brunner R. J., Richards G. T., Nichol R. C., Schneider D. P., Bahcall N. A., 2007, Astrophysical Journal, 658, 99

Myers A. D., Richards G. T., Brunner R. J., Schneider D. P., Strand N. E., Hall P. B., Blomquist J. A., York D. G., 2008, Astrophysical Journal, 678, 635

Nelson R. P., Papaloizou J. C. B., Masset F., Kley W., 2000, Mon. Not. R. Astron. Soc., 318, 18

Nixon C. J., Cossins P. J., King A. R., Pringle J. E., 2011, Mon. Not. R. Astron. Soc., 412, 1591

Papaloizou J., Pringle J. E., 1977, Mon. Not. R. Astron. Soc., 181, 441

Preto M., Berentzen I., Berczik P., Spurzem R., 2011, Astrophys. J. Lett., 732, L26+

Price D. J., 2007, Publ. Astron. Soc. Aust., 24, 159

Rice W. K. M., Lodato G., Armitage P. J., 2005, Mon. Not. R. Astron. Soc, 364, L56

Roedig C., Dotti M., Sesana A., Cuadra J., Colpi M., 2011, Mon. Not. R. Astron. Soc, 415, 3033

Sanders D. B., Mirabel I. F., 1996, Annual Review of Astronomy and Astrophysics, 34, 749

Shakura N. I., Sunyaev R. A., 1973, Astronomy & Astrophysics, 24, 337

Shen Y., Richards G. T., Strauss M. A., Hall P. B., Schneider D. P., Snedden S., Bizyaev D., Brewington H., Malanushenko V., Malanushenko E., Oravetz D., Pan K., Simmons A., 2011, Astrophys. J. Supplements, 194, 45

Shi J.-M., Krolik J. H., Lubow S. H., Hawley J. F., 2011, ArXiv e-prints

Springel V., 2005, Mon. Not. Roy. Astr. Soc., 364, 1105

Springel V., Di Matteo T., Hernquist L., 2005, Mon. Not. Roy. Astr. Soc., 361, 776

Volonteri M., Gültekin K., Dotti M., 2010, Mon. Not. Roy. Astr. Soc., 404, 2143

Ward W. R., 1997, Icarus, 126, 261

White S. D. M., Rees M. J., 1978, Mon. Not. R. Astron. Soc., 183, 341